Hydrogen atom transfer reactions of He^+ and Ne^+ with H_2, D_2, and HD

Kent M. Ervin[a] and P. B. Armentrout[b]
Department of Chemistry, University of California, Berkeley, California 94720

(Received 8 January 1987; accepted 27 February 1987)

The hydrogen atom transfer reactions of helium(1 +) and neon(1 +) ions with isotopic molecular hydrogen (H_2, D_2, and HD) are investigated using guided ion beam techniques. These reactions are exothermic, but are known to be extremely slow at thermal energies. The cross sections for formation of HeH^+ (HeD^+) and NeH^+ (NeD^+) exhibit thresholds at high relative translational energies, 8 to 12 eV c.m. Unusual isotope effects are observed in the reaction with HD. The deuteride product is formed exclusively near threshold, while the hydride product predominates at higher energies. Reaction mechanisms involving Rydberg excited states of HeH_2^+ and NeH_2^+ are discussed.

I. INTRODUCTION

The reactions of helium and neon ions with molecular hydrogen,

$$\begin{aligned}
He^+ + H_2 &\rightarrow HeH^+ + H, & \Delta H = -8.3\ \text{eV}, & \quad (1a)\\
&\rightarrow He + H^+ + H, & \Delta H = -6.4\ \text{eV}, & \quad (1b)\\
&\rightarrow He + H_2^+, & \Delta H = -9.2\ \text{eV}, & \quad (1c)\\
Ne^+ + H_2 &\rightarrow NeH^+ + H, & \Delta H = -5.6\ \text{eV}, & \quad (2a)\\
&\rightarrow Ne + H^+ + H, & \Delta H = -3.5\ \text{eV}, & \quad (2b)\\
&\rightarrow Ne + H_2^+, & \Delta H = -6.1\ \text{eV}, & \quad (2c)
\end{aligned}$$

are well-known examples of exothermic[1] ion–molecule reactions that react extremely slowly at thermal energies. The total reaction rate[2–6] for reaction (1) at 300 K is $\sim 1\times10^{-13}$ $cm^3\ s^{-1}$ and the rate[7–9] for reaction (2) is also small, $k<3\times10^{-13}$ $cm^3\ s^{-1}$. Both are four orders of magnitude smaller than the collision rates according to the Langevin–Gioumousis–Stevenson (LGS) model.[10] This behavior contrasts starkly with the hydrogen atom transfer reactions of argon[11] and krypton[12] ions with hydrogen, which proceed at approximately 70% and 20% of the LGS collision rates, respectively.

The experimental branching ratio for the helium reactions indicates that both H^+ and H_2^+ are produced, but there is no evidence of HeH^+ formation at low energies.[3,4,6,13,14] The branching ratio for the neon reactions is unknown.[15] At high relative collision energies, $E>9$ eV, Jones *et al.*[13] have observed the hydrogen atom transfer reaction, process (1a), as well as chemiluminescence from electronically excited hydrogen atoms. No such studies have been performed for the Ne^+ system.

The aim of the present work is to investigate the dynamics of the high energy process that leads to hydrogen atom transfer by determining the translational energy dependence and kinetic isotope effects of the reaction. Guided ion beam techniques are used to determine the absolute cross sections of reactions (1a) and (2a) as a function of the relative translational energy of the reactants up to 50 eV. We have recently reported studies of the analogous argon[11] and krypton[12] systems. The reactions with deuterium,

$$He^+ + D_2 \rightarrow HeD^+ + D, \quad (3)$$

$$Ne^+ + D_2 \rightarrow NeD^+ + D, \quad (4)$$

and with HD,

$$\begin{aligned}
He^+ + HD &\rightarrow HeH^+ + D, & \quad (5a)\\
&\rightarrow HeD^+ + H, & \quad (5b)\\
Ne^+ + HD &\rightarrow NeH^+ + D, & \quad (6a)\\
&\rightarrow NeD^+ + H, & \quad (6b)
\end{aligned}$$

are also examined. The results for reactions (1a) and (3) are compared with the relative cross sections obtained by Jones *et al.*[13] Observations of reactions (2a), (4), (5), and (6) are reported here for the first time. The isotopic branching of the reactions with HD is particularly useful in providing information on the underlying dynamics of the reactions.

A. Experimental and theoretical background

The basic reasons for the nonreactivity of He^+ and Ne^+ with hydrogen have been understood for some time. As outlined by Mahan[16] and Kuntz and Roach,[17] the observed behavior can be explained on the basis of electronic state correlations between reactants and products. Figure 1 presents the diatomic potential energy curves[18–21] for NeH_2^+ in the asymptotic $[Ne + H_2]^+$ reactant and $[NeH + H]^+$ product regions. Mahan[16] and Preston *et al.*[22] have presented the analogous curves for the helium system. Because the ionization potential of neon, IP(Ne) = 21.6 eV, is higher than that of molecular hydrogen, $IP(H_2) = 15.4$ eV, the $Ne^+ + H_2$ charge state is 6.2 eV higher than the ground charge state, $Ne + H_2^+$. The helium surfaces are qualitatively similar to the neon surfaces, except that IP(He) = 24.6 eV and consequently the $[X^+ + H + H]$ dissociation asymptote lies an additional 3 eV higher, relative to ground state $[X + H^+ + H]$. In both cases, the $X^+ + H_2$ charge state of reactants represents a high electronically excited state of the XH_2^+ system.

It is instructive to examine first the ground state surface of the XH_2^+ system, which corresponds to the $X + H_2^+$ charge state in the reactant region. As shown in Fig. 1, the dissociation asymptote of $X + H_2^+$ is $[X + H^+ + H]$, to

[a] Present address: Joint Institute for Laboratory Astrophysics, University of Colorado, Boulder, CO 80309-0440.
[b] N.S.F. Presidential Young Investigator 1984–1989; Alfred P. Sloan Fellow 1986–1988.

 0021-9606/87/116240-11$02.10

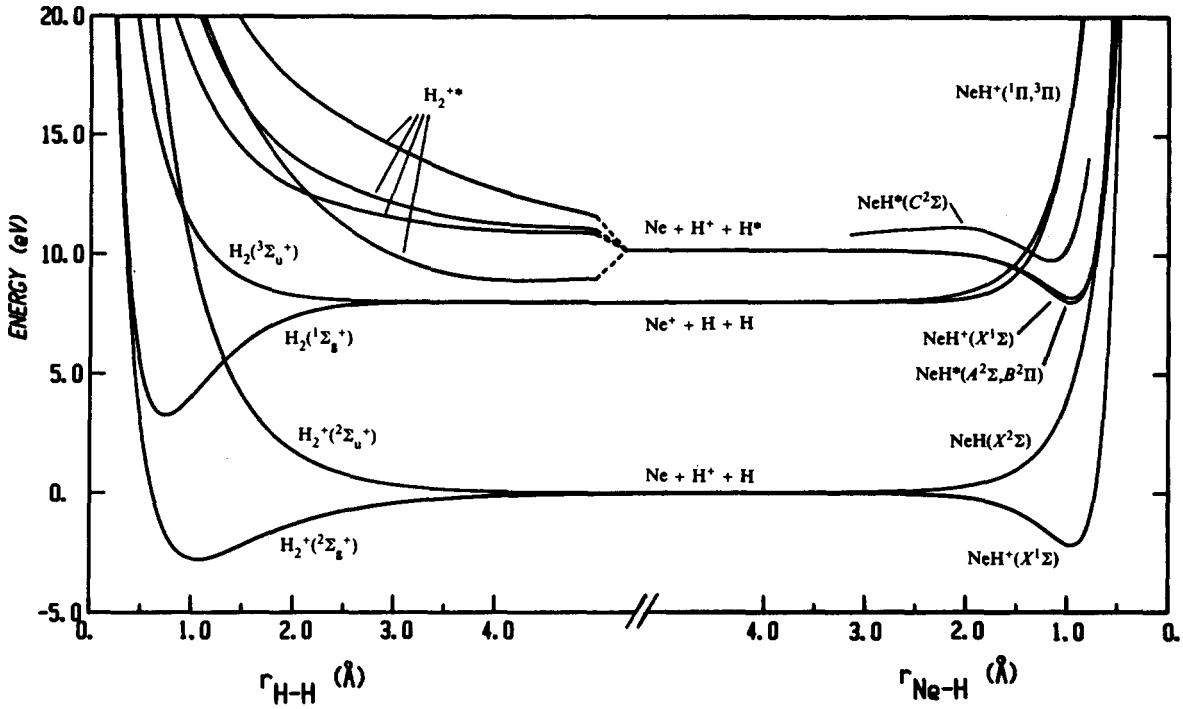

FIG. 1. Asymptotic potential energy curves for the NeH_2^+ system. The curves on the left represent the energies as a function of r(H–H) with r(Ne–H_2) = ∞ and the curves on the right represent the energies as a function of r(Ne–H) with r(NeH–H) = ∞.

which ground state $XH^+ + H$ products also dissociate. Kuntz and Roach[17] and Mahan[16] pointed out that these states correlate with one another, providing an adiabatic pathway for the reactions[1]

$$He + H_2^+ \rightarrow HeH^+ + H, \quad \Delta H = +0.81 \text{ eV}, \qquad (7)$$

and

$$Ne + H_2^+ \rightarrow NeH^+ + H, \quad \Delta H = +0.55 \text{ eV}. \qquad (8)$$

Experimental studies of reactions (7)[23] and (8)[24] have shown that they proceed efficiently once the endothermicity is supplied either as translational or as vibrational energy. *Ab initio* calculations of the ground state potential energy surfaces[25] and reaction dynamics calculations[26] have complemented the experimental studies.

Unlike the $X + H_2^+$ ground charge state, the $X^+ + H_2$ state leads to the $[X^+ + H + H]$ dissociation asymptote, which correlates with repulsive excited states of $[XH + H]^+$, Fig. 1. There is no adiabatic or diabatic path leading from $X^+ + H_2$ to ground state $XH^+ + H$ products, and, therefore, that reaction is impossible despite the large thermochemical driving force. As a result, reaction (1a) does not proceed to any detectable degree at low energies.[27]

The same diabatic correlations apply to the reactions of argon[11] and krypton[12] ions with hydrogen, which would suggest that they also should not proceed at low energies. For argon and krypton, however, the $X^+ + H_2$ and $X + H_2^+$ charge states of reactants have similar energies, and the two states cross near the equilibrium bond length of H_2. As Ar^+ or Kr^+ approaches hydrogen this crossing is avoided, forming two new adiabatic surfaces. The lower adiabatic surface leads to ground state ArH^+ or KrH^+ products with no energy barrier, and consequently the argon and krypton reactions proceed at a substantial fraction of the LGS collision cross section.[11,12] This adiabatic reaction pathway is absent in the helium and neon systems due to the large separation of the $X^+ + H_2$ and $X + H_2^+$ charge states.

Jones *et al.*[13] measured relative cross sections for reactions (1a) and (3) at high energies and observed thresholds of 9.0 ± 0.1 eV for both reactions. They also looked at chemiluminescence from the collisions of He^+ with molecular hydrogen and observed that the onset of Lyman-α radiation from excited hydrogen atom products, H*(2p), coincides with the threshold energy for reactions (1a) and (3). Jones *et al.*[13] inferred that HeH^+ or HeD^+ formation is possible only when the neutral product is an electronically excited hydrogen atom. These high energy processes must involve excited electronic states of HeH_2^+ that correlate with Rydberg levels of the separated atoms. Unfortunately, while the ground state HeH_2^+ and NeH_2^+ potential energy surfaces are well studied, there have been only limited calculations of excited state surfaces of the helium[22,28–31] and neon[20] systems.

At low energies, the observed product channels for the $He^+ + H_2$ reaction are reactions (1b) and (1c),[3,4,13] although the experimental branching ratio is a matter of some controversy.[32] The H^+/H_2^+ branching ratio is difficult to

measure directly because of the small total rate constant and because rapid secondary reactions of these ions with H_2 convert both products to H_3^+.[5] Although a number of measurements of the total rate or of one channel have been reported,[3-6,13,14] no single experiment has unambiguously measured both product channels simultaneously.

Mahan[16] pointed out that H^+ formation, reactions (1b) and (2b), can occur as a result of the crossing between the $X^+ + H_2(^1\Sigma_g^+)$ surface and the repulsive $X + H_2^+(^2\Sigma_u^+)$ surface, shown in Fig. 1 for X = Ne. As the rare gas ion approaches the hydrogen molecule, this crossing is avoided to form two adiabatic surfaces. However, the adiabatic coupling between the diabatic surfaces is expected to be small and there is an energy barrier to reach the crossing seam. A theoretical treatment by Preston *et al.*[22] shows that the dissociative reaction (1b) is possible via a tunneling mechanism and predicts that hydrogen vibrational energy should be particularly effective in promoting the reaction. Once on the repulsive $X + H_2^+(^2\Sigma_u^+)$ surface, the system quickly decomposes to $X + H^+ + H$ products. At low translational energies reaction (1b) is slow, but significant reaction is observed above 6 to 7 eV.[13,14,33] Ellison and co-workers[34] reported that vibrationally excited hydrogen reacts at 10% or more of the LGS collision rate with both Ne^+ and He^+ at thermal energies, a spectacular three or four orders of magnitude enhancement of the reaction probability.

Jones *et al.*[13] observed H_2^+ formation, reaction (1c), at low energies and Wu and Hopper[6] have measured the cross sections from near-thermal energies up to 60 eV c.m. An associative radiation mechanism for reaction (1c) at low energies has been proposed by Hopper.[6,30] This involves formation of a He^+–H_2 intermediate, which is bound only by the long-range polarization well, followed by radiative relaxation to the ground state He–H_2^+ surface and decomposition to $He + H_2^+$. The radiative step requires photon emission at a predicted wavelength of about 153 nm.[30] This emission has not been observed experimentally.

II. EXPERIMENTAL METHODS

The guided ion beam apparatus and data reduction procedures have been described in detail previously.[11,35] A brief outline of the experiment is included here.

Helium(1 +) and neon(1 +) ions are produced by electron impact ionization with electron energies below the threshold for formation of metastable Rydberg states, i.e., less than 65 and 48 eV, respectively.[36] Only the $^2S_{1/2}$ ground state of He^+ is present, but both $^2P_{3/2}$ (0.0 eV) and $^2P_{1/2}$ (0.097 eV) spin–orbit states of Ne^+ are produced, presumably with a 2:1 statistical population. Contamination by an impurity ion of mass 20 was encountered in preparation of the $^{20}Ne^+$ ion beam. This impurity was present in fractional intensities of 10^{-3} to 10^{-4} relative to Ne^+. The impurity species undergoes hydrogen atom transfer with H_2, D_2, and HD at low energies,[37] but has not been positively identified. The contamination could be avoided by using extra precautions to keep the ion source and gas handling system clean or by switching to the $^{22}Ne^+$ isotope (9.2% natural abundance).

The ions are extracted from the ion source, focused into a beam, and mass analyzed in a magnetic sector to select the desired species. The ions are then refocused and injected at the desired ion kinetic energy into a radio-frequency octopole ion beam guide. The octopole, which passes through the gas collision cell, creates a radial potential well along the axis of the ion beam which traps ions in radial directions but does not affect their axial velocities. The radial trapping field serves to collect scattered product ions efficiently. This greatly improves the sensitivity compared to conventional beam/gas cell instruments and avoids artifacts due to different collection efficiencies for product ions scattered in different directions.

Neutral reactant densities are kept low enough that multiple ion–molecule collisions are improbable. Product ions and unreacted primary ions drift to the end of the octopole, are extracted from it, mass analyzed with a quadrupole mass filter, and detected by secondary electron scintillation and pulse-counting electronics. The reaction cross sections are derived directly from the reactant and product ion intensities, the gas cell pressure, and the estimated reaction path length.[11,35]

The absolute kinetic energy of the ion beam is measured to within ± 0.10 eV lab by utilizing the octopole itself as a retarding field energy analyzer.[11,35] For this purpose, the ion intensity is measured while the sweeping the DC potential of the octopole through the nominal ion energy zero, the difference between the octopole DC potential and the ion source anode potential. The ion beam energy and its distribution are determined by fitting a Gaussian distribution to the retarding potential curve. Because the energy analysis region and the reaction zone are physically the same, ambiguities in the energy analysis resulting from contact potentials, space charge effects, and focusing aberrations are minimized. Laboratory ion energies are converted to center-of-mass (c.m.) frame energies using the usual stationary target assumption.[11,35] The ion energy distributions produced by the electron impact source described above are typically 0.4 eV lab [0.13 eV c.m. for reaction (1) and 0.04 eV c.m. for reaction (2)].

III. RESULTS

A. Cross section determinations

Experimental cross sections for the hydrogen atom transfer reactions of He^+ and Ne^+ with H_2, HD, and D_2 are presented in Figs. 2–7. The data for each reaction represent averages of several determinations performed at different times over the course of two years. Because the measured cross sections are extremely small, the experimental uncertainties are larger than are typically cited for the guided ion beam technique.[11,35] Based on statistical uncertainties and the reproducibility of the results, we estimate that for the Ne^+ reactions the relative error of the cross sections is within 20% and the error in the absolute magnitudes is within 50%.

The He^+ reactions are more difficult to study since the apparatus is not optimized in several respects for collection and detection of low-mass products. First, the frequency of

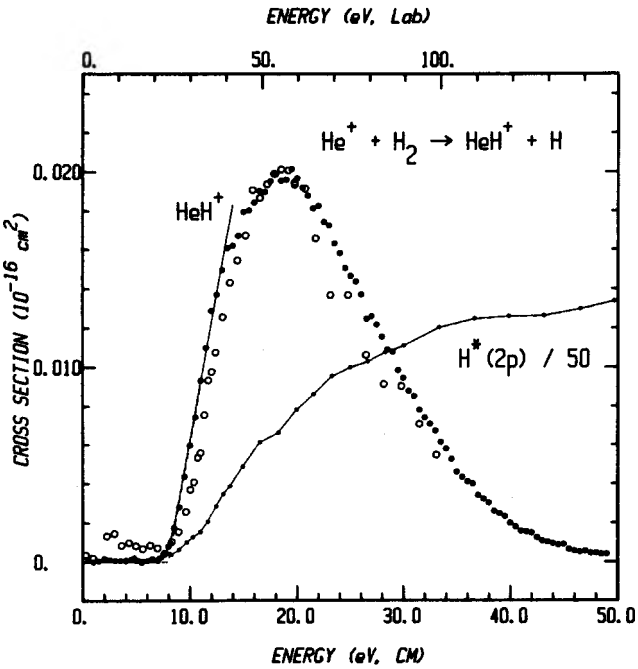

FIG. 2. Experimental cross section for reaction (1a), solid circles, as a function of the ion energy in the laboratory frame (upper scale) and center-of-mass frame (lower scale). The relative cross sections of Jones *et al.* (Ref. 13), open circles, are scaled in magnitude to match the present results. The connected points represent the cross section (reduced by a factor of 50) for Lyman-α chemiluminescence from Jones *et al.* The solid line is the linear threshold model described in the text, convoluted over the experimental energy distributions. The unconvoluted model, which differs from the convoluted form only very near the threshold, is shown as a dashed line.

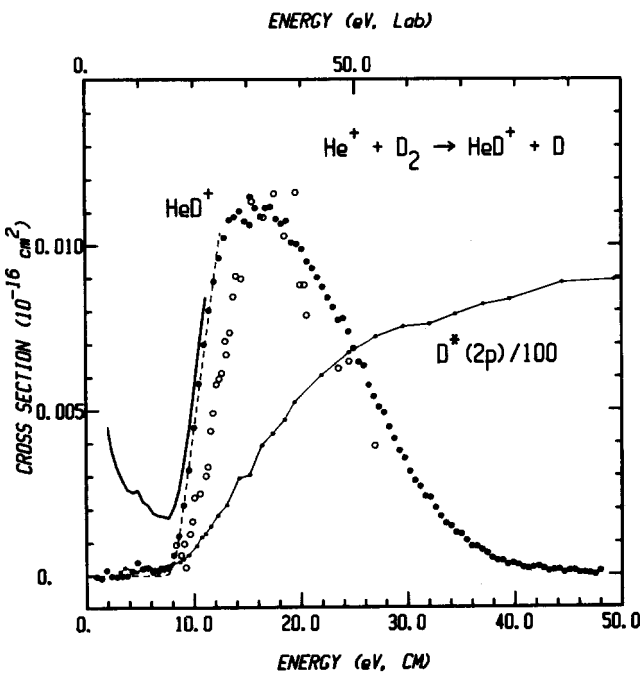

FIG. 3. Experimental cross section for reaction (3), solid circles, corrected for secondary reactions at low energies as described in the text. The solid curve is the uncorrected cross section at a high D_2 pressure. The relative cross sections of Jones *et al.* (Ref. 13), open circles, are scaled in magnitude to match the present results. The connected points represent the cross section (reduced by a factor of 100) for Lyman-α chemiluminescence from Jones *et al.* The dashed line is the linear threshold model described in the text, convoluted over the experimental energy distributions.

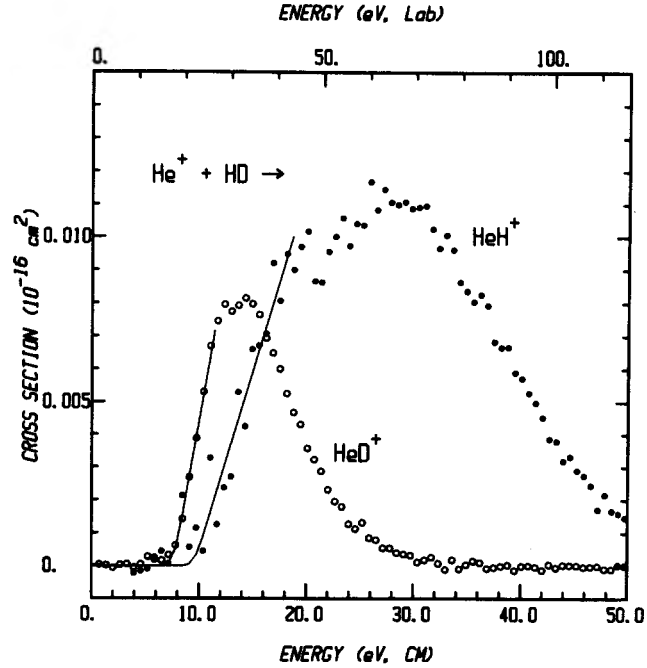

FIG. 4. Experimental cross sections for reactions (5a), solid circles, and (5b), open circles, corrected for secondary reactions at low energies as described in the text. The lines are the linear threshold model described in the text, convoluted over the experimental energy distribution.

the radio-frequency trapping potential on the octopole ion beam guide must be high to trap low-mass ions without subjecting them to high-frequency oscillations. In these studies, the highest instrumentally available frequency, ~13 MHz,

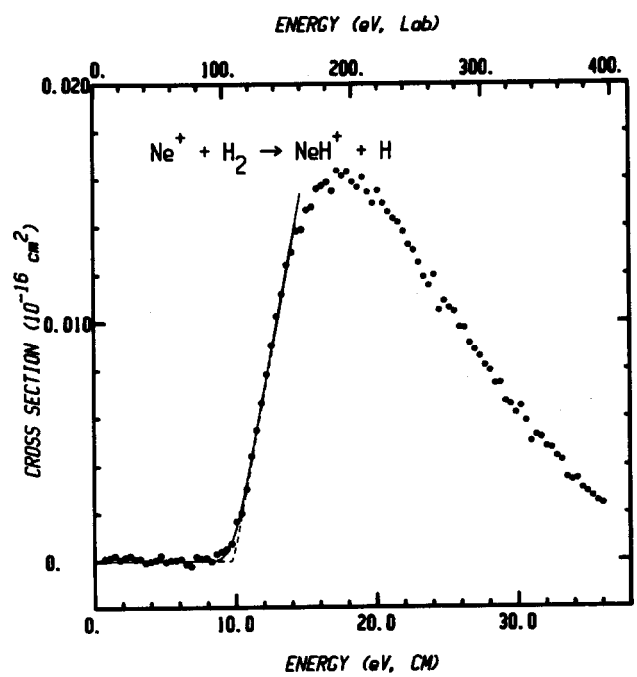

FIG. 5. Cross section for reaction (2a), points, as a function of the ion energy in the laboratory frame (upper scale) and the center-of-mass frame (lower scale). The dashed line is the linear threshold model described in the text and the solid line is this model convoluted over the experimental energy distribution.

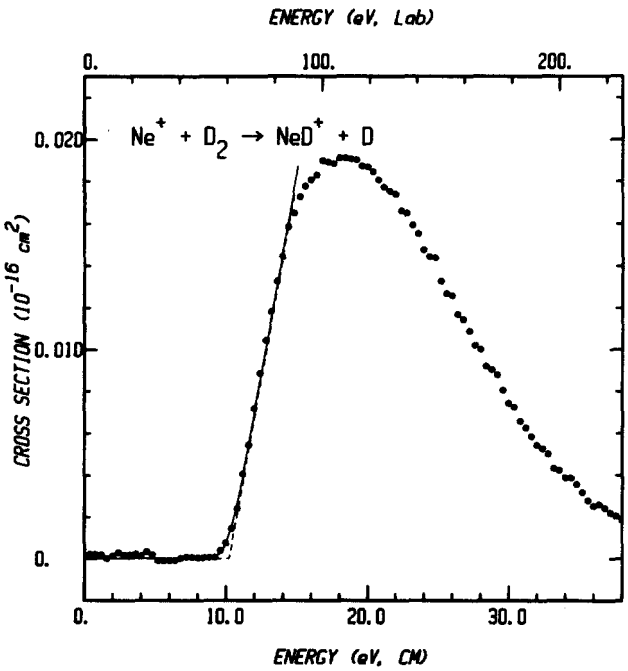

FIG. 6. Cross section for reaction (4), points, as a function of the ion energy in the laboratory frame (upper scale) and the center-of-mass frame (lower scale). The dashed line is the linear threshold model described in the text and the solid line is this model convoluted over the experimental energy distribution.

was used, but higher frequencies may be optimal. While we cannot rule out the possibility of ion losses, no dependence of the cross sections on the octopole trapping potential is observed. A second problem involves the quadrupole mass filter in the detection system. The measured transmission of ions through the final quadrupole mass filter is independent of mass above 10 amu,[11,35] but quadrupoles are prone to discriminate against low masses. The highest available quadrupole frequency, ~5.6 MHz, was used to limit this effect. No mass corrections have been applied to the data. Despite the problems in measurement of the He^+ reaction cross sections, we estimate their magnitudes are accurate to within a factor of 2.

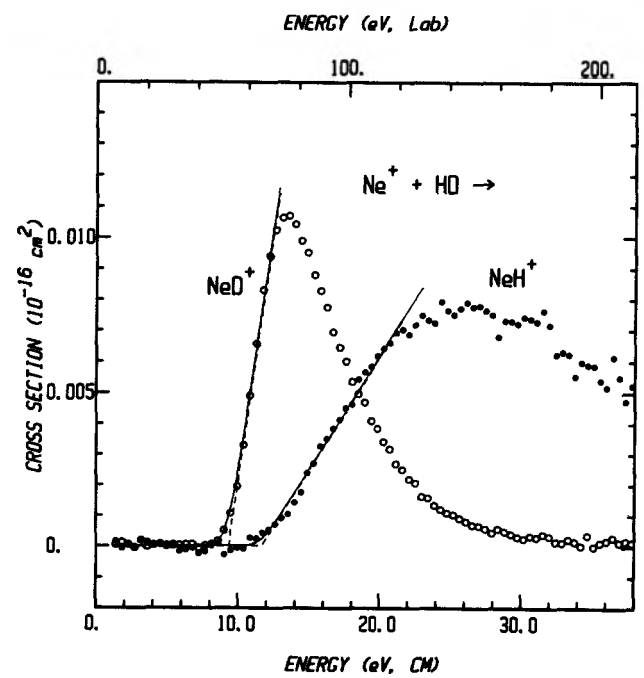

FIG. 7. Experimental cross sections for reactions (6a), solid circles, and (6b), open circles, as a function of the ion energy in the laboratory frame (upper scale) and the center-of-mass frame (lower scale). The dashed lines are linear threshold models, described in the text, and the solid lines show these models convoluted over the experimental energy distribution.

B. Other reaction channels and secondary reactions

No attempt was made to measure the cross sections for the H^+ and H_2^+ product channels, for the following reasons. First, the problems with low-mass ion detection mentioned above apply to these products. Second, it is difficult to resolve H^+ products (1 amu) from the background since all masses are transmitted by the quadrupole mass filter at the zero mass setting. Third, charge transfer products can be formed with low momentum transfer and therefore can have small forward velocities in the laboratory frame. Such slow ions are inefficiently transmitted through the quadrupole mass filter and have a reduced detection probability. Finally and most importantly, the following secondary reactions interfere with the direct measurement of the H^+ and H_2^+ product channels:

$$H^+ + H_2 \rightarrow H_2^+ + H, \quad (9)$$

$$H_2^+ + H_2 \rightarrow H_3^+ + H. \quad (10)$$

Process (9) is endothermic, $\Delta H = 1.8$ eV, which for most systems would exclude it from consideration as a secondary process, but it may be significant here since H^+ may be formed with high kinetic energies, according to the dissociative charge transfer mechanism described in the introduction. Reaction (10) is definitely significant because it is very rapid, $k \simeq 1.4 \times 10^{-9}$ cm^3 s^{-1},[38] and because relatively high H_2 pressures (up to 1.0 mTorr) are used in order to measure the small cross sections for formation of HeH^+. Furthermore, since charge transfer products can be formed in processes with low momentum transfer, they can remain trapped in the octopole interaction region for a long time as they drift towards the detector, allowing extensive conversion of H_2^+ to H_3^+ to take place. In a conventional beam/gas cell apparatus, such slow products would drift out of the interaction region in random directions and would have a low probability of detection. Thus, the trapping of the octopole beam guide actually promotes secondary reactions of charge transfer products.

The secondary reactions have impeded other experimental determinations of the branching ratio for reactions (1b) and (1c) at low energies.[3-5,32] In principle, the high sensitivity and wide energy range of the guided beam technique ideally suit it for an investigation of reactions (1b), (1c), (2b), and (2c), but alterations of the detection system of the present apparatus would be required to permit accurate measurement of the low-mass products and of products with low laboratory frame kinetic energies. Neglecting the

H^+ and H_2^+ product channels, however, introduces no significant errors in the determination of the hydrogen atom transfer cross sections.

Secondary reaction products impose an additional experimental difficulty for the helium reactions. The trihydrogen ion secondary products interfere with reaction (3) because of the mass overlap of HeD^+ and D_3^+ (6 amu) and with reaction (5a) because of the overlap of HeH^+ and HD_2^+ (5 amu). The secondary products appear as low-energy channels, below the threshold energies expected by comparison to reactions (1a) and (5b). The latter reactions exhibit no low-energy channels since the secondary product ion masses do not overlap with the primary product masses. The low-energy features in the apparent cross sections of reactions (3) and (5a) are dependent on pressure, as expected for secondary processes. This is shown in Fig. 8, which shows the apparent cross sections for reaction (5a) at several HD reactant gas pressures. The pressure-dependent part of the cross section includes an exothermic component and a feature that peaks at about 18 eV. Unfortunately, because of low signal levels it is not possible to go to low enough pressures to obtain a clean extrapolation to zero pressure. Instead, we estimate the energy dependence of the pressure dependent component from measurements at a high hydrogen pressure, scale this at low energies to the measurements at lower pressure, and subtract it out to obtain the cross section due only to HeH^+ or HeD^+. The result for reaction (5a) is shown in Fig. 8 as well as in Fig. 4; Fig. 3 shows the result of a similar correction for reaction (3). The correction is not strictly valid since it arbitrarily assumes that there is no primary reaction in the low energy region and that the pressure dependence is identical at all energies. Therefore, the behavior of reactions (3) and (5a) in the threshold regions is uncertain. Nevertheless, the qualitative behavior of the cross sections is unambiguous from the raw data and by comparison to the other isotopic reactions.

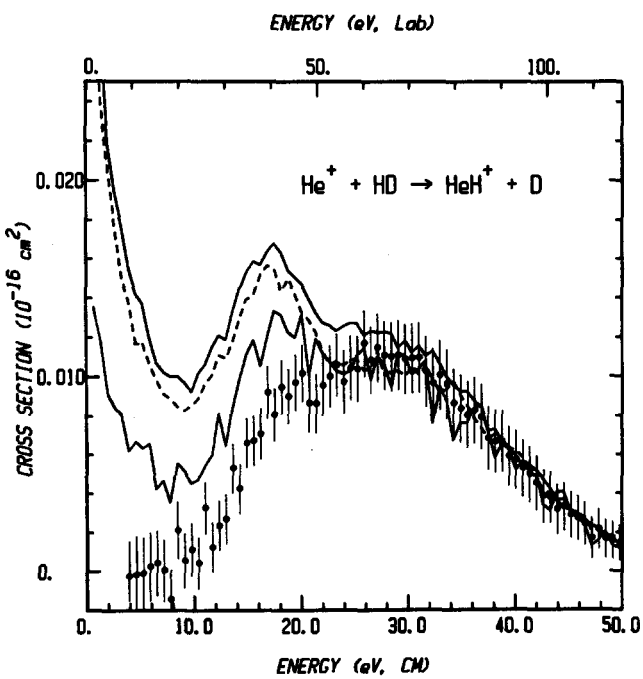

FIG. 8. Effect of secondary reactions of the apparent cross section for reaction (5a). The lines represent the apparent cross sections at three HD pressures: upper solid curve, 1.0 mTorr; dashed curve, 0.4 mTorr; lower solid curve, 0.05 mTorr. The points represent these curves corrected to exclude the secondary product, D_2H^+, as discussed in the text. Error bars represent $\pm$ 2 standard deviations of the extrapolated values.

C. Comparison to previous measurements

The relative cross sections for reactions (1a) and (3) reported by Jones *et al.*[13] are plotted in Figs. 2 and 3 for comparison to the present data. Their relative cross section values are scaled to the present absolute cross sections at the peaks. The relative behavior of the cross sections are in good qualitative agreement.

D. Threshold energies

Each of the hydrogen atom transfer reactions, Figs. 2–7, exhibit high apparent thresholds. The threshold behavior of the reactions is modeled using a simple linear threshold law,

$$\sigma(E) = \sigma_0 \cdot (E - E_T), \quad \text{if } E > E_T,$$
$$\sigma(E) = 0, \quad \text{if } E \leqslant E_T, \tag{11}$$

where $\sigma(E)$ is the model cross sections as a function of the relative energy, E_T is the threshold energy, and σ_0 is an energy-independent scaling factor. The parameters σ_0 and E_T in Eq. (11) are optimized to fit the data after convolution over the experimental energy distribution, using procedures described elsewhere.[11,35] The optimized fits are compared to the data in Figs. 2–7. At the high energies of the apparent thresholds, the energy broadening is a relatively minor effect. Other functional forms of the cross section, such as the hard-sphere line-of-centers model[39] and the ion-induced dipole model,[40,41] can fit the data only over a more limited energy range above the threshold. The threshold energies obtained from the linear threshold model are presented in Table I, along with uncertainties based on the variance among fits to independent sets of data. The error limits for the thresholds of reactions (3) and (5a) are large because of the uncertainty introduced by subtraction of secondary product channels.

Jones *et al.*[13] obtained threshold energies of 9.0 ± 0.1 eV for both reactions (1a) and (3), compared to our results of $E_T = 8.1 \pm 0.3$ eV for reaction (1a) and $E_T = 8.2 \pm 1$ eV for reaction (3), Table I. It seems unlikely that this deviation [$\sim$1 eV c.m. or 3 eV lab for reaction (1) and 2 eV lab for reaction (3)] is due to errors in the energy determinations. The relative cross sections of Jones *et al.* exhibit a nonzero baseline below the apparent thresholds for reaction (1a), which suggests that the true onset may have been masked by background signals. This could cause a kinetic shift, that is, push the apparent threshold to higher energies. For reaction (3) Jones *et al.* do not present baseline data below the threshold region. Since the magnitudes of the cross sections near the apparent thresholds for the present data are close to the detection limit of our apparatus (about 2×10^{-20} cm^2 for the ion intensities, reactant gas pressures, and background

TABLE I. Threshold energies (eV).[a]

Reaction	X = He		X = Ne	
	E_{cm}	E_p	E_{cm}	E_p
$X^+ + H_2 \rightarrow XH^+ + H$	8.1 ± 0.3	4.9 ± 0.2	9.8 ± 0.2	4.7 ± 0.1
$X^+ + D_2 \rightarrow XD^+ + D$	8.2 ± 1	5.5 ± 0.7	10.2 ± 0.2	5.6 ± 0.1
$X^+ + HD \rightarrow XH^+ + D$	9.6 ± 1	4.5 ± 0.5	11.7 ± 0.4	4.3 ± 0.2
$X^+ + HD \rightarrow XD^+ + H$	7.7 ± 0.3	6.0 ± 0.2	9.4 ± 0.2	6.6 ± 0.1

[a] Threshold energy optimized to fit the data for the linear threshold model, Eq. (11). E_{cm}, center-of-mass frame energy scale; E_p, pairwise energy scale, Eq. (14).

count rate under the conditions of these experiments), we cannot definitely rule out kinetic shifts in our threshold determinations. Thus, thresholds in Table I are strictly upper limits to the true thermodynamic endothermicity of reaction.

IV. DISCUSSION

The experimental cross sections, Figs. 2–7, exhibit the following major features: (1) The reactions have high apparent thresholds, 8 to 12 eV, despite the large exothermicities. (2) The cross sections are extremely small, peaking at values of 1 to 2×10^{-18} cm^2 (0.01 to 0.02 Å^2). (3) The reactions with HD show a striking and unusual isotope effect, with XD^+ produced exclusively near the threshold and the XH^+ product appearing at higher energies. (4) The results for the helium and neon systems are remarkably similar with regard to the cross sections magnitudes, energetics, and isotope effects.

The hard-sphere cross section, given by $\sigma = \pi R^2$, with R roughly estimated by $r_e(XH^+) + r_e(H_2)/2$, is 5.8 Å^2 for X = Ne and 4.1 Å^2 for X = He.[42] Thus, reactions take place only on one of every ~300 collisions at the peak of the cross sections.[43] Both the high threshold energies and the low reaction probabilities indicate that the mechanism for hydrogen atom transfer in these reactions is extremely inefficient. In the following, the reaction energetics, isotope effects, and known features of the potential energy surfaces are examined to shed light on the reaction mechanism.

A. Reaction energetics

The observed threshold energies, 8 to 12 eV c.m. (Table I), exceed the strengths of any of the chemical bonds in the XH_2^+ system and correspond to about twice the energy required for simple collision induced dissociation,

$$X^+ + H_2 \rightarrow X^+ + H + H, \quad \Delta H = 4.5 \text{ eV}. \tag{12}$$

The total available energy at the measured thresholds, including the translational energy and the reaction exothermicity (i.e., the available electronic energy) for ground state $XH^+ + H$ products, is 16.3 eV for reaction (1a) and 15.6 eV for reaction (2a).

To form stable diatomic products, the excess energy must be deposited either in relative translational energy of the $XH^+ + H$ products or in electronic energy of the products. The observation by Jones *et al.*[13] of chemiluminescence from electronic excited hydrogen atoms in $He^+ + H_2$ and $He^+ + D_2$ collisions establishes that electronic excitation of the atomic hydrogen product occurs in the helium system. Figures 2 and 3 include the cross sections of Jones *et al.* for Lyman-α radiation, which comes from the relaxation of $H^*(2p)$ to ground state $H(1s)$. $H^*(2s)$ excited hydrogen atoms have the same energy and are probably formed also, but they cannot be observed because radiative relaxation to the ground state is forbidden. As shown in Figs. 2 and 3, the apparent thresholds for Lyman-α chemiluminescence correspond exactly with the HeH^+ and HeD^+ thresholds. Jones *et al.* pointed out that this correlation strongly suggests that the two processes occur concomitantly, that is, by the process

$$X^+ + H_2 \rightarrow XH^+ + H^*(n = 2). \tag{13}$$

Based on the other strong similarities between the helium and neon systems, we would predict that NeH^+ is also formed via process (13).

Assuming that $H^*(n = 2)$ excited hydrogen atoms are formed in process (13) at threshold, the reaction enthalpies are $\Delta H = +1.9$ eV for X = He and $\Delta H = +4.6$ eV for X = Ne. The observed translational energy thresholds are still considerably larger than these endoergicities, giving excess energies ($E_T - \Delta H$) of 6.1 eV for reaction (1a) and 5.4 eV for reaction (2a). This still represents a substantial amount of energy which must be distributed among the translational and internal modes of the products. Diatomic product vibration can account for only a part of this available energy since the dissociation energies are $D_0(HeH^+) = 1.85$ eV and $D_0(NeH^+) = 2.10$ eV.[1] Further electronic excitation of the products can also be excluded, at least near the observed thresholds, since (1) the observed threshold for production of $H^*(n > 2)$ in the helium case is several electron volts higher [12.2 ± 1.0 eV c.m. for Balmer-α radiation from $H^*(n = 3)$[13]] and (2) the lowest bound electronically excited states of HeH^+ and NeH^+ are Rydberg levels which lie at much higher energies. By elimination, the excess energy must appear as kinetic energy of the XH^+ and H^* products.

The relative magnitudes of the present cross sections for

HeH^+ or HeD^+ production and the Lyman-α chemiluminescence cross sections of Jones *et al.*,[13] compared in Figs. 2 and 3, indicate that the diatomic product is formed only in a small fraction (and possibly none) of the collisions resulting in H* production. Apparently, only a few collision trajectories can lead to HeH^+ that is stable to dissociation, i.e., without too much internal energy. It may be more realistic to think of the hydrogen atom transfer mechanism in terms of a collision induced dissociation process in which the $[He + H]^+$ products sometimes happen to be scattered with relative energies smaller than the HeH^+ binding energy. While the chemiluminescence has not been measured for the neon system, similar considerations are probably applicable.

B. Isotope effects

The extremely strong isotope effects exhibited by the reactions with HD, Figs. 4 and 7, can be immediately interpreted as indicating a direct, impulsive (i.e., hard-sphere-like) reaction mechanism. A statistical process, or any mechanism involving strong interactions among all three atoms, would give much closer to equal amounts of the two isotopic product channels. Furthermore, the striking differences in the energy dependence of the XH^+ and XD^+ channels shows that the mechanism depends strongly on the mass of the transferred atom.

A comparison of the threshold energies in Table I shows that the thresholds for formation of XD^+ products from HD are lower than the thresholds for the H_2 and D_2 reactions, while the thresholds for XH^+ from HD are higher. One may conclude from these large threshold shifts that the observed activation energies do not correspond to a real potential energy barrier. If that were the case, the thresholds for all isotopic channels would be the same except for vibrational zero-point energy differences, which are negligible on the scale of Figs. 2–7. The peaks of the cross sections exhibit similar energy shifts for the various isotopic reactions. The cross sections for reactions of both He^+ and Ne^+ with H_2 and D_2 peak at 17–19 eV, while the cross sections for XD^+ from $X^+ + HD$ peak at ~ 13 eV and the cross sections for XH^+ from $X^+ + HD$ peak at 24–28 eV. The strong kinetic isotope effects observed for reactions (5) and (6) can be viewed as shifts in the energy scales of the reactions. In other words, the center-of-mass energy scale does not represent the energy which is available to drive the reactions.

The energy shifts for the isotopic reactions are in the direction predicted by a model for impulsive, pairwise interactions which has been described previously.[12,44] For the general reaction $A + BC \rightarrow AB + C$, this model assumes the collision occurs primarily between the ion A and atom B in the target molecule. Atom C is largely a spectator. The relative energy available in a pairwise interaction depends only on the masses of A and B. This pairwise energy is reduced from the total center-of-mass energy according to

$$E_p = E_{cm} \cdot M \cdot m_B / (m_A + m_B) \cdot (m_B + m_C) , \quad (14)$$

where m_x is the mass of atom X and $M = m_A + m_B + m_C$. In the reaction with HD, E_p is greater if B = D than if B = H. This qualitatively explains why the XD^+ cross sections are shifted to lower energies compared to XH^+ in reactions (5) and (6). According to Eq. (14), E_p for reaction with H_2 and D_2 are nearly the same and are intermediate between E_p for HD (B = H) and HD (B = D). This is also in qualitative agreement with the observed energy shifts for reactions (1a), (2a), (3), and (4) relative to reactions (5) and (6).

The threshold energies for the hydrogen atom transfer reactions are given in Table I on the pairwise energy scale, according to Eq. (14), in addition to the center-of-mass energy scale. The thresholds for the HD reaction on the pairwise energy scale are reversed compared to the center-of-mass threshold energies, indicating that the mass factor in Eq. (14) overcorrects for the observed threshold shifts and thus that the pairwise interaction model does not account for the energy shifts quantitatively. The relative energies of the peaks of the cross sections more closely follow that predicted by the pairwise interaction model. On the pairwise energy scale, the peaks occur at 11 to 12 eV for the helium reactions and at 9 to 10 eV for the neon reactions. While the pairwise energy scale does not completely describe the isotopic variation of reaction energetics, the overall cross section behavior suggests that the mechanism is related to this simple pairwise, impulsive interaction model. An impulsive, high-energy reaction mechanism can predominate in systems where chemical interactions at lower energies are repulsive. The behavior of the potential energy surface is discussed in the following section.

C. Potential energy surfaces

According to the diatomic potential energy curves presented in Fig. 1, the $XH^+ + H^*$ products correlate asymptotically with Rydberg states of $X + H_2^{+*}$. The mechanism for $XH^+ + H^*$ formation, process (13), must involve transitions to excited electronic states of XH_2^+ that correlate to the Rydberg states of products. While all approaches of the $X^+ + H_2$ reactants are repulsive, molecular orbital considerations suggest that a near-collinear approach is the least repulsive orientation. Figure 9 presents an electronic state correlation diagram which summarize the available information about the potential energy surfaces in the interaction region for collinear $NeHH^+$. The helium system will be considered later.

Correlations between the separated atom and the diatomic $[Ne + H_2]^+$ reactant and $[NeH + H]^+$ products states are on the left-hand and right-hand sides of Fig. 9, respectively. These correlations are comparable to the asymptotic diatomic potential energy curves in Fig. 1. In the center are shown the diabatic correlations between the reactant and product states and collinear $NeHH^+$ states. The relative energies of the $NeHH^+$ states are taken from the calculations of Vasudevan[20] for the geometry $r(Ne–H) = r(H–H) = 2.3$ bohr, near the equilibrium geometry of ground state $NeHH^+$. As $Ne^+(^2P)$ and $H_2(^1\Sigma_g^+)$ approach collinearly, repulsive $^2\Sigma$ and $^2\Pi$ states of $NeHH^+$ are formed. Vasudevan's calculations identified avoided crossings, denoted by circles in Fig. 9, between these states and $^2\Sigma$ and $^2\Pi$ states which correlate with $[NeH + H]^+$ product states. The $^2\Sigma$ reactant surface has an avoided crossing with

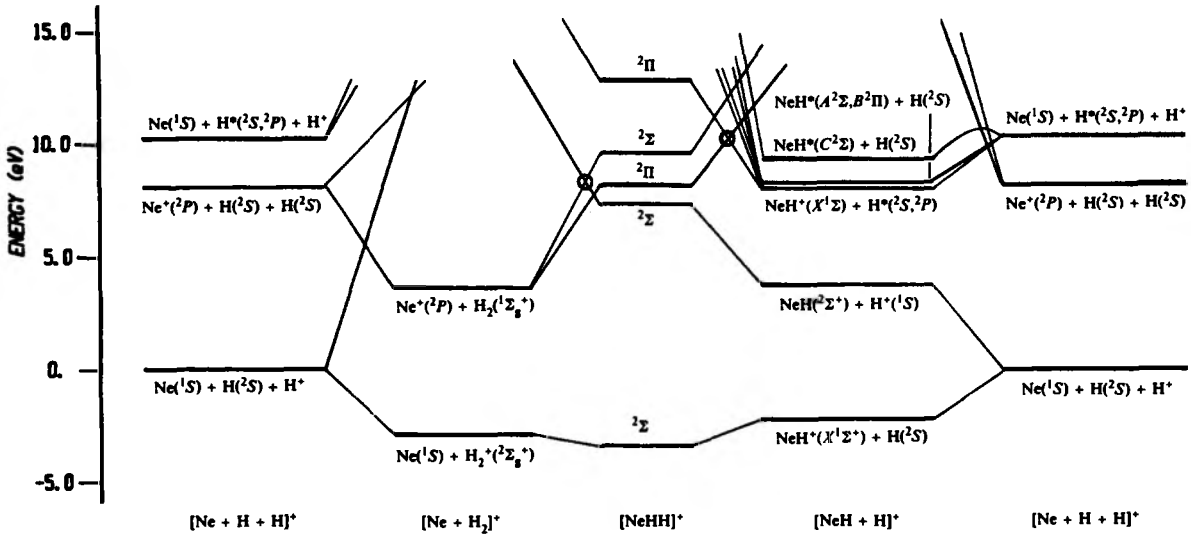

FIG. 9. Electronic state correlation diagram for $NeHH^+$ in collinear $C_{\infty v}$ symmetry.

the repulsive $NeH(X\,^2\Sigma^+) + H^+$ state. The $^2\Pi$ surface from $Ne^+ + H_2$ has an avoided crossing with a $^2\Pi$ surface which leads to $NeH^+(X\,^1\Sigma) + H^*(n=2)$ products.

When the collinear $C_{\infty v}$ symmetry is relaxed to general C_s symmetry, the $^2\Sigma$ states become $^2A'$ and the $^2\Pi$ states split into $^2A'$ and $^2A''$ components. The $^2\Sigma(^2A')$ and $^2\Pi(^2A'',^2A')$ avoided crossings (Fig. 9) are preserved, while additional avoided crossings arise between $^2\Pi(^2A')$ and $^2\Sigma(^2A')$ surfaces. Thus both $^2A'$ surfaces from $Ne^+ + H_2$ have avoided crossings with the $^2\Sigma(^2A')$ repulsive state of $NeH + H^+$, which decomposes to $Ne + H^+ + H$. If a transition to this surface occurs, the overall process is dissociative charge transfer, reaction (2b). At higher energies, the $^2A'$ states have additional avoided crossings with the $^2A'(^2\Pi)$ state leading to $NeH^+ + H^*$ products. The $^2A''(^2\Pi)$ surface of reactants has its lowest avoided crossing with the $^2A''(^2\Pi)$ surface of $NeH^+ + H^*$.

These avoided crossings with the $^2A'$ and $^2A''$ surfaces of $NeH^+ + H^*$ surface can account for the observed behavior of the hydrogen atom transfer reactions. First, the neutral product is electronically excited hydrogen atom, as is inferred from the experimental results, process (13). Second, the barrier height is consistent with the observed threshold energies. Based on the previous discussion of the reaction energetics and isotope effects, the actual potential energy barrier to hydrogen atom transfer processes probably lies somewhere above the threshold energies on the pairwise energy scale [4.5–6.5 eV (see Table I)], but below the lowest center-of-mass threshold energy [i.e., 7.7 ± 0.3 eV from reaction (5b) for helium and 9.4 ± 0.2 eV from reaction (6b) for neon]. The energy at the avoided crossing to $NeH^+ + H^*$ is about 6.5 eV above reactants according to Vasudevan's calculations.[20] This is consistent with the observed reaction energetics, although the actual barrier height may be somewhat different since Vasudevan considered only collinear geometries with r(Ne–H) fixed at 2.3 bohr.

Third, the NeH^+–H^* repulsion on the surface leading to products will promote kinetic energy release into the products, thus providing a mechanism for depositing the excess available energy into product translation and stabilizing the NeH^+ diatom against dissociation. Finally, the extremely small reaction cross sections are consistent with a low probability of transitions to the $NeH^+ + H^*$ surface. The adiabatic coupling between the surfaces at the avoided crossing, and therefore the transition probability, is small because both surfaces are repulsive and because the transitions involve two-electron changes in molecular orbital configuration.[20] Thus, most collisions passing through the crossing region will behave diabatically and will not make the transition which leads to product formation. As noted above, the $^2A'$ surfaces from reactants have avoided crossings (also with weak coupling) with $NeH + H^+$ at lower energies, which reduces the probability that trajectories on these surfaces ever reach the region of interaction with $NeH^+ + H^*$.

There are a number of higher-energy crossings between the $^2\Sigma(^2A')$ and $^2\Pi(^2A',^2A'')$ surfaces of $NeHH^+$ and surfaces arising from $NeH^+ + H^*$ and the nearly-degenerate Rydberg states $NeH^*(^2\Pi,^2\Sigma) + H^+$ (Fig. 9). Crossings between those surfaces that have the same symmetry will be avoided, although the locations and orderings of the crossings are uncertain. These crossings can lead to hydrogen atom transfer products and also suggest a high energy pathway for formation of H^+ with a NeH^* Rydberg state as the neutral product. Trajectories involving transitions at these higher-energy crossings, however, are probably less likely to form stable diatomic products.

The correlation diagram for the HeH_2^+ is similar to the one for NeH_2^+, with two main qualitative differences between the neon and helium systems. First, the states corre-

lating to $[X^+ + H + H]$ separated atoms lie about 3 eV higher, relative to the $[X + H^+ + H]$ and $[X + H^+ + H^*]$ asymptotes, for X = He than for X = Ne. This places $[He^+ + H + H]$ about 1 eV above $[He + H^+ + H^*]$, but does not alter the overall correlations between reactants and products. Second, while $Ne^+(^2P) + H_2(^1\Sigma)$ forms both $^2\Sigma(^2A')$ and $^2\Pi(^2A', ^2A'')$ surfaces, $He^+(^2S) + H_2(^1\Sigma)$ forms only a $^2\Sigma(^2A')$ surface. Therefore, the $^2\Pi$ surface correlating with reactants for the neon system, shown in Fig. 9, is not present for helium. However, both $^2\Sigma$ and $^2\Pi$ surfaces are produced by combinations of $[HeH + H]^+$ product states. The crossing of the $^2\Sigma(^2A')$ surface of $He^+ + H_2$ reactants with the $^2\Sigma(^2A')$ surface leading to $HeH + H^+$ can be avoided, as can the higher-energy crossing with the $^2\Pi(^2A')$ surface of $HeH^+ + H^*$. The behavior of these avoided crossings is expected to be similar to those in the neon system (i.e., the adiabatic coupling is weak), and the mechanism for reaction (13) discussed above for the neon system applies to the helium system as well. To reach $HeH^+ + H^*$ products, however, the system must pass through the region of the first avoided crossing on the $^2A'$ surface without making a transition to the dissociative $HeH + H^+$ surface.

Hopper[30] has constructed a correlation diagram for HeH_2^+ which mainly refers to the H^+ and H_2^+ product channels and does not include the crossings with the Rydberg states that lead to $HeH^+ + H^*$ products. Hopper placed the avoided crossing leading to dissociative charge transfer, analogous to the $^2\Sigma$ crossing circled in Fig. 9, at ~7 eV above reactants, based on the experimental threshold[13] for that process. However, the present experiments show that the center-of-mass threshold energies for this system do not necessarily correspond to the potential energy barrier heights, and the actual position of this avoided crossing is probably lower than 7 eV.

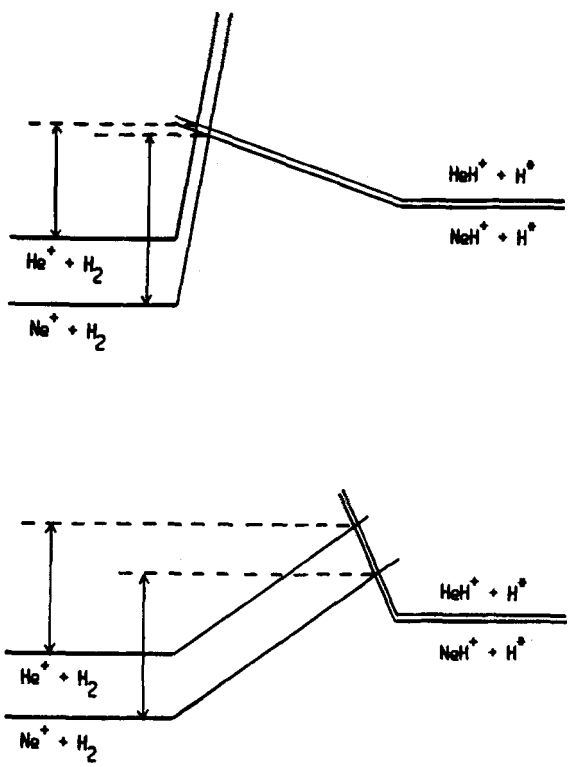

FIG. 10. Schematic curve crossings which explain the dependence of the barrier heights of the two rare gas systems on the surface topology in the crossing region. At the top are curve crossings which lead to barrier heights which are different from each other by nearly their asymptotic energy differences. On the bottom, the barrier heights are about the same despite the differences in the asymptotic energies.

It is interesting to compare the threshold energies for the helium and neon systems. On the pairwise energy scale, the thresholds for corresponding isotopic reactions (Table I) are the same within experimental error for helium and neon [with the exception of reactions (5b) and (6b), for which the difference is only 0.6 ± 0.3 eV]. The reaction enthalpies for the He^+ and Ne^+ reactions differ by 2.7 eV. This is nearly the difference between the ionization potentials IP(He) = 24.6 eV and IP(Ne) = 21.6 eV, since the $He–H^+$ and $Ne–H^+$ bond energies are similar. The similar threshold energies for the helium and neon systems implies that the barrier height has little dependence on the energy levels of $XH^+ + H^*$ product states. This would be the case if, at the curve crossing, the surfaces that correlate to $XH^+ + H^*$ are much steeper than the surfaces that correlate to the $X^+ + H_2$. Figure 10 shows schematic depictions of curve crossings to explain this effect. This interpretation is speculative, however, because the two-dimensional view of the curve crossings in Fig. 10 is clearly oversimplified and the detailed behavior of the potential energy surfaces in the crossing regions is unknown.

V. SUMMARY

In this study, the hydrogen atom transfer reaction cross sections of collisions of He^+ and Ne^+ with H_2, D_2, and HD have been measured. Only the reactions of He^+ with H_2 and D_2 have been observed previously.[13]

The behavior of the helium and neon systems is quite similar. The reactions are characterized by high energy thresholds, small reaction probabilities, and extreme isotope effects in the reactions with HD. The isotope effects indicate that the reaction mechanism is impulsive and largely between individual atoms, rather than involving three-body interactions. The products are formed with large relative kinetic energies. Comparisons with chemiluminescence experiments[13] for $He^+ + H_2$ and D_2 suggest that hydrogen atom transfer occurs concomitantly with excited hydrogen atom production, $H^*(n \geqslant 2)$. Although no chemiluminescence studies have been performed for the neon system, a similar process is likely. The mechanism for this reaction involves crossings of potential energy surfaces of high electronic states of HeH_2^+ and NeH_2^+ that correlate with $HeH^+ + H^*$ and $NeH^+ + H^*$ excited states of products.

ACKNOWLEDGMENT

This research was supported by the National Science Foundation, Grant No. CHE-8608847.

[1]Reaction enthalpies are derived from tabulated bond energies [K. Huber and G. Herzberg, *Constants of Diatomic Molecules* (Van Nostrand Reinhold, New York, 1979)] and ionization potentials [H. M. Rosenstock, K.

Draxl, B. W. Steiner, and J. T. Herron, J. Phys. Chem. Ref. Data **6**, Suppl. 1 (1977)]. The bond energy $D_0^\circ(\text{Ne–H}^+) = 2.10 \pm 0.03$ eV is from J. Lorenzen, H. Hotop, M.-W. Ruf, and H. Morgner, Z. Phys. A **297**, 19 (1980).

[2]F. C. Fehsenfeld, A. L. Schmeltekopf, P. D. Goldan, H. I. Schiff, and E. E. Ferguson, J. Chem. Phys. **44**, 4087 (1966).

[3]R. Johnsen and M. A. Biondi, J. Chem. Phys. **61**, 2112 (1974).

[4]R. Johnsen, A. Chen, and M. A. Biondi, J. Chem. Phys. **72**, 3085 (1980).

[5]H. Böhringer and F. Arnold, J. Chem. Phys. **84**, 1459 (1986).

[6]R. L. C. Wu and D. G. Hopper, Chem. Phys. **57**, 385 (1981).

[7]R. S. Hemsworth, R. C. Boldern, M. J. Shaw, and N. D. Twiddy, Chem. Phys. Lett. **5**, 237 (1970).

[8]A. B. Rakshit and N. D. Twiddy, Chem. Phys. Lett. **60**, 400 (1979).

[9]R. D. Smith, D. L. Smith, and J. H. Futrell, Int. J. Mass Spectrom. Ion Phys. **19**, 369 (1976).

[10]G. Gioumousis and D. P. Stevenson, J. Chem. Phys. **29**, 294 (1958).

[11]K. M. Ervin and P. B. Armentrout, J. Chem. Phys. **83**, 166 (1985); see citations therein for further information on the $Ar^+ + H_2$ system.

[12]K. M. Ervin and P. B. Armentrout, J. Chem. Phys. **85**, 6380 (1986); see citations therein for further information on the $Kr^+ + H_2$ system.

[13]E. G. Jones, R. L. C. Wu, B. M. Hughes, T. O. Tiernan, and D. G. Hopper, J. Chem. Phys. **73**, 5631 (1980).

[14]D. G. Hopper and R. L. C. Wu, Chem. Phys. Lett. **81**, 230 (1981).

[15]Rakshit and Twiddy (Ref. 8) reported that reaction (2) was at or below their detection limit, $k \leqslant 3.2 \times 10^{-13}$, and that the products were 100% NeH^+.

[16]B. H. Mahan, J. Chem. Phys. **55**, 1436 (1971); Acc. Chem. Res. **8**, 55 (1975).

[17]P. J. Kuntz and A. C. Roach, J. Chem. Soc. Faraday Trans. 2 **68**, 259 (1972).

[18]R. L. Matcha, M. B. Milleur, and P. F. Meier, J. Chem. Phys. **68**, 4748 (1978).

[19]V. Bondybey, P. K. Pearson, and H. F. Schaefer III, J. Chem. Phys. **57**, 1123 (1972).

[20]K. Vasudevan, Mol. Phys. **30**, 437 (1975).

[21]Potential energy curves for NeH^+, NeH, and NeH* are taken from Refs. 18, 19, and 20. The ground and first excited state curves of H_2 and H_2^+ are generated from the modified Morse potentials given by Ref. 17. The H_2^+* Rydberg state curves are taken from D. R. Bates, K. Ledsham, and A. L. Stewart, Philos. Trans. R. Soc. London, Ser. A **246**, 215 (1953).

[22]R. K. Preston, D. L. Thompson, and D. R. McLaughlin, J. Chem. Phys. **68**, 13 (1978).

[23]W. A. Chupka and M. E. Russell, J. Chem. Phys. **49**, 5426 (1968); J. A. Rutherford and D. A. Vroom, *ibid.* **58**, 4076 (1973); R. H. Neynaber and G. D. Magnuson, *ibid.* **59**, 825 (1973); V. Pacak, U. Havemann, Z. Herman, F. Schneider, and L. Zülicke, Chem. Phys. Lett. **49**, 273 (1977); U. Havemann, V. Pacak, Z. Herman, F. Schneider, Ch. Zuhrt, and L. Zülicke, Chem. Phys. **28**, 147 (1978); T. Turner, O. Dutuit, and Y. T. Lee, J. Chem. Phys. **81**, 3475 (1984); M. Baer, S. Suzuki, K. Tanaka, I. Koyano, H. Nakamura, Z. Herman, and D. J. Kouri, Phys. Rev. A **34**, 1748 (1986).

[24]R. M. Bilotta and J. M. Farrar, J. Chem. Phys. **75**, 1776 (1981); D. Van Pijkeren, J. Van Eck, and A. Niehaus, Chem. Phys. Lett. **96**, 20 (1983); D. Van Pijkeren, E. Boltjes, J. Van Eck, and A. Niehaus, Chem. Phys. **91**, 293 (1984).

[25]P. J. Brown and E. F. Hayes, J. Chem. Phys. **55**, 922 (1971); C. Edmiston, J. Doolittle, K. Murphy, K. C. Tang, and W. Wilson, *ibid.* **52**, 3419 (1970); E. F. Hayes, A. K. Q. Siu, F. M. Chapman, Jr., and R. L. Matcha, *ibid.* **65**, 1901 (1976); F. Schneider, L. Zülicke, R. Polak, and J. Vojtik, Chem. Phys. **76**, 259 (1983).

[26]W. N. Whitton and P. J. Kuntz, J. Chem. Phys. **64**, 3624 (1976); N. Sathyamurthy, R. Rangarajan, and L. M. Raff, *ibid.* **64**, 4606 (1976); F. Schneider, U. Havemann, L. Zülicke, and Z. Herman, Chem. Phys. Lett. **48**, 439 (1977); C. Stroud, N. Sathyamurthy, R. Rangarajan, and L. M. Raff, *ibid.* **48**, 350 (1977); C. Leforestier, *ibid.* **51**, 132 (1977); N. Sathyamurthy, J. W. Duff, C. Stroud, and L. M. Raff, J. Chem. Phys. **67**, 3563 (1977); C. Stroud and L. M. Raff, Chem. Phys. **46**, 313 (1980); N. Sathyamurthy, *ibid.* **62**, 1 (1981).

[27]The cross section is less than 6×10^{-21} cm^2 between 0.13 and 7.5 eV [M. Schindler, Diplom-thesis, Universität Freiburg (1983), as cited in Ref. 5].

[28]D. R. McLaughlin and D. L. Thompson, J. Chem. Phys. **70**, 2748 (1979).

[29]F. Schneider and L. Zülicke, Chem. Phys. Lett. **67**, 491 (1979).

[30]D. G. Hopper, J. Chem. Phys. **73**, 3289, 4528 (1980); **74**, 4218 (1981).

[31]C. Kubach, C. Courbin-Gaussorgues, and V. Sidis, Chem. Phys. Lett. **119**, 523 (1985).

[32]R. Johnsen and M. A. Biondi, J. Chem. Phys. **74**, 6996 (1981); D. G. Hopper, *ibid.* **74**, 6997 (1981).

[33]R. W. Rozette and W. S. Koski, J. Chem. Phys. **48**, 533 (1968).

[34]M. E. Jones, S. E. Barlow, G. B. Ellison, and E. E. Ferguson, Chem. Phys. Lett. **130**, 218 (1986).

[35]Kent M. Ervin, Ph.D. thesis, University of California, Berkeley (1986).

[36]C. E. Moore, *Atomic Energy Levels*, Natl. Bur. Stand. Ref. Data Ser. Natl. Bur. Stand., Vol. 1., No. 35 (U.S. GPO, Washington, D.C., 1970).

[37]In presentation of preliminary work (K. M. Ervin and P. B. Armentrout, Conference on the Dynamics of Molecular Collisions, Snowbird, UT, July 1985), we mistakenly attributed the impurity cross section to a small (< 0.002 Å^2) exothermic channel for the $Ne^+ + H_2$ reaction.

[38]M. T. Bowers, D. D. Elleman, and J. King, Jr., J. Chem. Phys. **50**, 4787 (1969).

[39]R. D. Levine and R. B. Bernstein, *Molecular Reaction Dynamics* (Oxford University, New York, 1974), p. 46.

[40]R. D. Levine and R. B. Bernstein, J. Chem. Phys. **56**, 2281 (1972).

[41]K. M. Ervin and P. B. Armentrout, J. Chem. Phys. **84**, 6738 (1986).

[42]Equilibrium bond lengths r_e are tabulated in K. Huber and G. Herzberg, *Constants of Diatomic Molecules* (Van Nostrand Reinhold, New York, 1979).

[43]The collision cross section according to the LGS model (Ref. 10) for the ion-induced dipole long-range potential is ~ 3 Å^2 at 20 eV for reactions with hydrogen, but the LGS model is not valid at such high energies.

[44]J. L. Elkind and P. B. Armentrout, J. Chem. Phys. **84**, 4862 (1986); J. Phys. Chem. **90**, 5736 (1986).